

Lindblad-driven quarkonium production in heavy-ion collisions

Néstor Armesto^a, Miguel Ángel Escobedo^b, Elena G. Ferreiro^a, Víctor López-Pardo^a

^a*Instituto Galego de Física de Altas Enerxías IGFAE, Universidade de Santiago de Compostela, Rúa de Xoaquín Díaz de Rábago, s/n, Santiago de Compostela, 15782, Galicia, Spain*

^b*Departament de Física Quàntica i Astrofísica and Institut de Ciències del Cosmos, Universitat de Barcelona, Martí i Franquès 1, Barcelona, 08028, Catalonia, Spain*

Abstract

We study the production of the conventional quarkonium states in ultrarelativistic heavy-ion collisions using an open quantum system framework based on the Lindblad equation. Starting from the complex-valued in-medium potential, we derive the dissociation temperature and thermal decay width for each state, and compute their survival probabilities for a system undergoing Bjorken expansion. We then extend the framework to include recombination from thermalized charm and bottom quarks in the quark-gluon plasma, deriving a coalescence model for quarkonia from the Lindblad equation under the adiabatic approximation. The methodology provides a unified, first-principles-inspired description of suppression and recombination for both charmonium and bottomonium.

Keywords: Quarkonium states, coalescence, heavy-ion collisions, finite temperature

1. Introduction

Heavy quarkonium states have long served as precision probes of the quark-gluon plasma (QGP) formed in ultrarelativistic heavy-ion collisions [1, 2]. The interplay of Debye screening of the heavy-quark potential and in-medium decoherence leads to a suppression of quarkonium yields that is ordered hierarchically with binding energy: the more weakly bound the state, the lower the temperature at which it dissolves in the plasma.

On the theoretical side, a significant advance has been the recognition that the in-medium heavy-quark potential is a complex-valued quantity [3, 4]: the real part exhibits Debye screening while the imaginary part encodes Landau damping of the mediating gluons. A systematic and phenomenologically successful parametrization of this potential is provided by the Gauss law model of Lafferty and Rothkopf [5], which combines the Cornell potential in vacuum with Hard-Thermal-Loop (HTL) perturbation theory for the medium response, reproducing nonperturbative lattice QCD results for both $\text{Re } V$ and $\text{Im } V$ with a single temperature-dependent parameter, the Debye mass m_D .

A complementary line of development treats quarkonium as an open quantum system coupled to the QGP bath [6, 7, 8, 9]. In this formalism the evolution of the density matrix of the heavy-quark pair is governed by a Lindblad equation, and the survival probability of a pre-formed bound state can be expressed in terms of the imaginary part of the complex potential. More recently, we have shown that the same framework also provides a natural coalescence model obtained by projecting the stochastic jumps of the Lindblad equation onto the bound-state subspace [10, 11]. Applied to the exotic state $X(3872)$, assumed to be a compact tetraquark, this approach predicted a sizable en-

hancement of the nuclear modification factor R_{AA} arising from recombination, compatible with CMS observations [12].

The goal of the present work is to apply this unified suppression-plus-recombination framework to the conventional quarkonium ground states. The paper is organized as follows. In Section 2 we recall the Gauss law complex potential and its parametrization. In Section 3 we derive the in-medium spectral functions for charmonium and bottomonium and we extract the binding energies, the thermal decay widths and the dissociation temperatures for J/ψ , $\psi(2S)$ and $\Upsilon(nS)$. In Section 4 we present the survival probability under Bjorken expansion derived within the recombination model from the Lindblad equation. Section 5 collects the phenomenological inputs and presents results for R_{AA} . Section 6 contains our conclusions and outlook.

2. In-medium potential

The starting point is the well-established Cornell form of the vacuum heavy-quark potential [13]:

$$V_{\text{vac}}(r) = -\frac{\tilde{\alpha}_s}{r} + \sigma r + c, \quad (1)$$

where $\tilde{\alpha}_s = C_F g^2/(4\pi)$ is the strong coupling including the Casimir factor C_F , σ is the string tension, and c is an additive renormalization constant. This potential captures both asymptotic freedom at short distances and linear confinement at large distances.

The parameters $\tilde{\alpha}_s$, $\sqrt{\sigma}$, and c could be fixed independently for the charmonium and bottomonium systems but, assuming the heavy quark potential is universal since at lowest order in pNRQCD the same expressions arise for both heavy quark families, we will fix the values for bottomonium and tune the charm

mass to reproduce the J/ψ and $\psi(2S)$ masses. The renormalon-subtracted bottom quark mass $m_b^{RS'} = 4.882$ GeV [14] is used for the bottomonium sector, while the charm mass $m_c^{\text{fit}} = 1.4692$ GeV reproduces the J/ψ and $\psi(2S)$ masses. The resulting parameters, common to Ref. [5], are: $\tilde{\alpha}_s = 0.513 \pm 0.002$, $\sqrt{\sigma} = 0.412 \pm 0.004$ GeV and $c = -0.161 \pm 0.003$ GeV.

At finite temperature the vacuum potential is modified by the QGP medium. The in-medium potential is written as

$$V(r, T) = \text{Re } V(r, m_D(T)) + i \text{Im } V(r, m_D(T)), \quad (2)$$

where r is the heavy quark-antiquark separation and $m_D(T)$ the Debye screening mass that encodes color screening in the QGP.

The real part of the in-medium potential is obtained by applying a linear-response (polarization/permittivity) procedure to the vacuum potential. Using the HTL permittivity $\varepsilon(p, m_D)$ according to $V(p) = V_{\text{vac}}(p)/\varepsilon(p, m_D)$ and enforcing smooth matching to the vacuum potential for $m_D \rightarrow 0$, one obtains

$$\begin{aligned} \text{Re } V(r, m_D(T)) = & -\tilde{\alpha}_s \left(m_D + \frac{e^{-m_D r}}{r} \right) + c \\ & + \sigma \left[\frac{2}{m_D} (1 - e^{-m_D r}) - r e^{-m_D r} \right], \end{aligned} \quad (3)$$

which reproduces the HTL result for the Coulomb term and the known string-term expression [5].

The imaginary part of the potential arises from Landau damping and the scattering of the heavy quark with medium gluons, which induces a finite in-medium width. While the Coulomb term of the imaginary part matches the HTL result, the string term needs to be regularized. Following [5] it is possible to rigorously remove the nonphysical divergence. The imaginary part of the quarkonium potential can then be written as

$$\text{Im } V(r, m_D(T)) = -\tilde{\alpha}_s T \phi(m_D r) + \frac{\sigma T}{m_D^2} \chi(m_D r, \Delta_D), \quad (4)$$

with

$$\chi(x, \Delta_D) = 2 \int_0^\infty du \frac{2 - 2 \cos ux - ux \sin ux}{\sqrt{u^2 + \Delta_D^2} (u^2 + 1)^2}. \quad (5)$$

Choosing the regularization constant to be $\Delta_D \simeq 3.0369$, the string term has a similar behavior to the Coulomb term at large distances since $\lim_{x \rightarrow \infty} \chi(x, \Delta_D) = 1$. Thanks to the regularization, the imaginary part of the potential is constant at large distances and high temperatures. This imaginary part is related to the decay width.

The behaviour of both the real and imaginary parts of the potential are shown in Figures 1 and 2.

3. In-medium spectral functions and dissociation properties

In the potential model approach, the in-medium quarkonium eigenenergies can be obtained by solving the Schrödinger equation with the complex potential. However, for a potential with

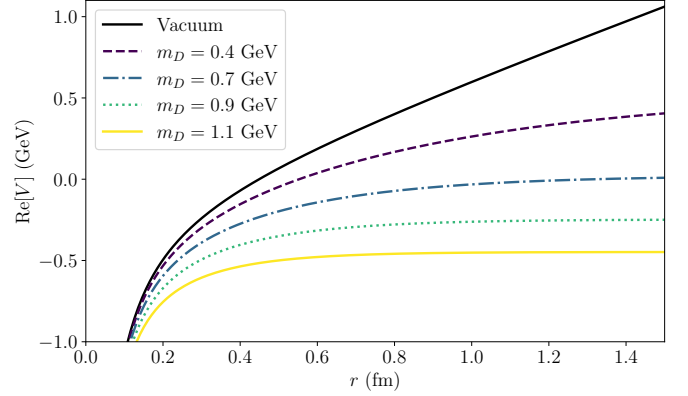


Figure 1: Real part of the in-medium potential for quarkonia as given by (3). It is clear that the increase in temperature (and Debye mass) makes the potential barrier smaller.

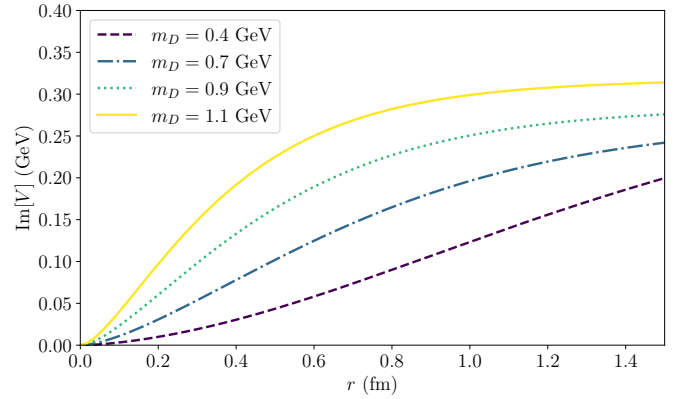


Figure 2: Imaginary part of the in-medium potential for quarkonia as given by (4). Only finite temperature cases are shown since the vacuum potential is purely real.

position-dependent imaginary part, the time-space solution of the Schrödinger equation becomes challenging since schemes used for Hermitian Hamiltonians, like Numerov's method used in [10, 11], become inapplicable. Nevertheless, the diagonalization of the Hamiltonian is possible and simpler in the frequency domain. The in-medium spectral functions are obtained by solving the frequency-space Schrödinger equation with the complex potential and extracting the imaginary part of the corresponding Green's function, which directly yields the quarkonium spectral shape, including both bound-state peaks and their thermal broadening [15].

Specifically, the spectral function is obtained as the imaginary part of the traced retarded Green's function of the Schrödinger equation with the complex potential,

$$\rho(\omega) = -\frac{1}{\pi} \text{Im} \int d^3 r G^R(r, r; \omega), \quad (6)$$

where $G^R(r, r'; \omega) = \langle r | (\omega + i\epsilon - H)^{-1} | r' \rangle$ and H contains the complex in-medium potential $V(r, T)$.

In the vicinity of each peak, when the decay width is a per-

turbation, the spectral function is well approximated by a Breit-Wigner distribution,

$$\rho(\omega) \approx \frac{1}{\pi} \frac{\Gamma_n/2}{(\omega - E_n)^2 + (\Gamma_n/2)^2}, \quad (7)$$

where E_n is the peak position and Γ_n is the full width at half maximum. In practice and following [5], the binding energy of each state is determined by identifying E_n with the in-medium mass and subtracting the sum of the constituent quark masses, while the thermal decay width is read off directly as the width of the peak measured at half of its maximum height. Since the spectral peaks are in general asymmetric, we do not fit a symmetric Breit-Wigner directly to the numerical spectral function. Instead, we employ a skewed Breit-Wigner profile, which better captures the distortion of the line shape near the continuum threshold and allows for a more reliable extraction of both E_n and Γ_n across the full temperature range.

3.1. Charmonium

The charmonium spectral function at various temperatures, displayed in Figure 3, exhibits two peaks at finite temperature.

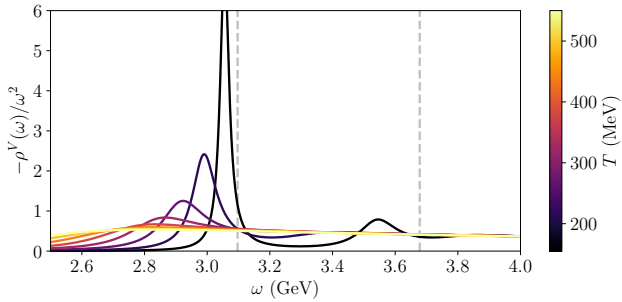


Figure 3: In-medium S -wave spectral functions for vector channel charmonium for different temperatures. The dashed gray vertical lines represent the $T = 0$ bound states J/ψ and $\psi(2S)$.

As the temperature increases, these peaks gradually shift toward lower frequencies and eventually fade away. At the same time, they become broader and less pronounced, indicating a shorter lifetime of the states. In the vacuum, the spectral function reduces to two Dirac delta functions located at the masses of the J/ψ and $\psi(2S)$, shown as dashed gray lines in the figure. By fitting the regions around the peaks with a skewed Breit-Wigner function one can extract how both the binding energy and decay width depend on temperature. The binding energy is determined from the peak position, interpreted as the in-medium mass, after subtracting the masses of the two constituent quarks. The decay width is given by the width of the peak measured at half of its maximum height.

The binding energy obtained with this method is shown in Figure 4. From this figure, it is evident that the binding energy of the J/ψ state can be tracked over nearly the entire temperature range, whereas the corresponding signal for the $\psi(2S)$ state is barely visible. This is due to the fact that the fit parameters of the $\psi(2S)$ spectral function cannot be reliably extracted

for temperatures $T \gtrsim 155$ MeV. As observed in Figure 3, the $\psi(2S)$ peak essentially disappears for all temperatures except the lowest one. In contrast, the binding energy of the J/ψ decreases steadily with increasing temperature, in agreement with the mass shift observed in Figure 3.

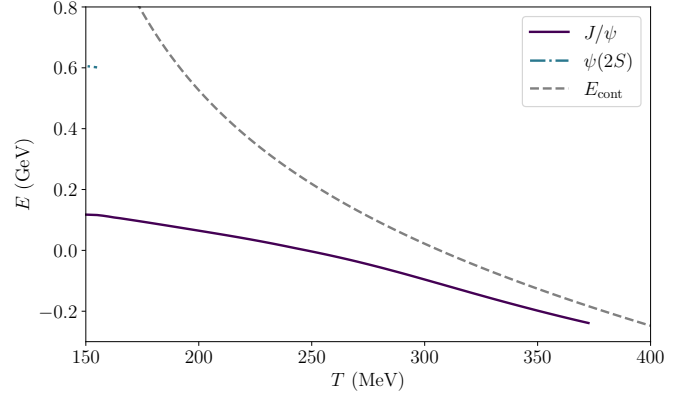


Figure 4: Binding energy for the different species of charmonium at finite temperature: J/ψ (solid purple line) and $\psi(2S)$ (dash-dot blue line). The potential barrier is also shown (dashed gray line). The $\psi(2S)$ line can barely be seen because the corresponding peak disappears at $T \gtrsim 155$ MeV.

The widths of the peaks shown in Figure 3 correspond to the decay widths of the charmonium states and are presented in Figure 5. As in the case of the binding energy, the $\psi(2S)$ peak is difficult to resolve, and therefore its decay width can only be reliably extracted for temperatures below 155 MeV. On the other hand, the J/ψ peak remains well defined over a much broader temperature range, allowing its decay width to be determined across a wide interval. Eventually, the J/ψ state dissociates, meaning that the corresponding peak disappears. Beyond this point, the notion of a decay width loses its meaning, and consequently it is no longer displayed in Figure 5.

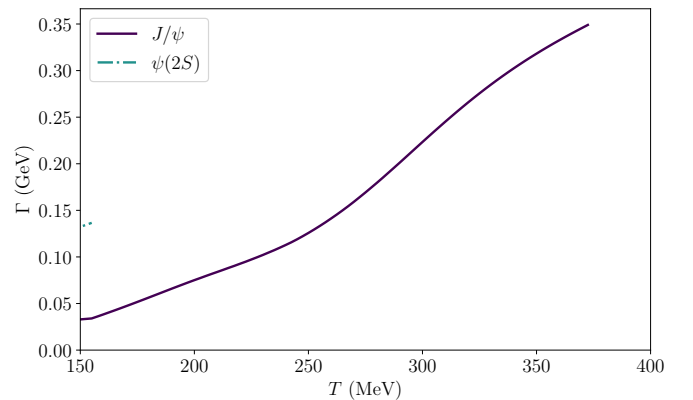


Figure 5: Decay width for the different species of charmonium at finite temperature: J/ψ (solid purple line) and $\psi(2S)$ (dash-dot blue line). The $\psi(2S)$ line is barely visible because the corresponding peak vanishes at $T \gtrsim 155$ MeV.

The dissociation temperature T_d is defined as the temperature above which the Schrödinger equation no longer admits

a bound-state solution, meaning that the corresponding spectral peak merges into the continuum. Equivalently, T_d can be identified as the temperature at which the in-medium binding energy vanishes. In practice, the dissociation temperature can be estimated from the spectral function as the highest temperature at which a distinct peak is still visible in Figure 3. This corresponds, in turn, to the last temperature point at which the given charmonium state appears in Figures 4 and 5. Using this approach, the dissociation temperatures of charmonium states are found to be approximately

$$T_{J/\psi} \approx 372 \text{ MeV}, \quad T_{\psi(2S)} \lesssim 155 \text{ MeV}.$$

These values are physically reasonable: the $\psi(2S)$, being weakly bound, dissociates at relatively low temperatures and barely survives in the medium, whereas the more tightly bound J/ψ persists up to higher temperatures.

3.2. Bottomonium

The bottomonium spectral function is obtained following the same procedure as in the charmonium case. As shown in Figure 6, increasing the temperature leads to a shift of the bottomonium peaks towards lower frequencies, accompanied by a broadening. The dashed gray lines indicate the Dirac delta functions corresponding to the spectral function in the vacuum. Although four S -wave states are present at zero temperature, only three of them remain at finite temperature. As in the char-

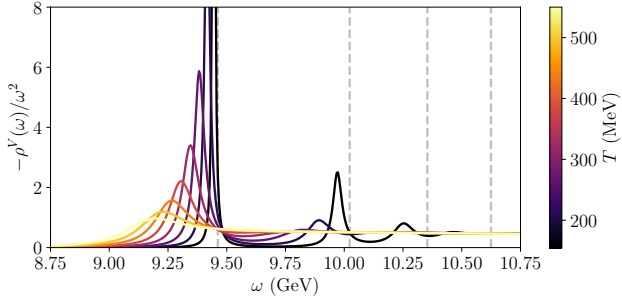


Figure 6: In-medium S -wave spectral functions for vector channel bottomonium for different temperatures. The dashed gray vertical lines represent the $T = 0$ bound states: $\Upsilon(1S)$, $\Upsilon(2S)$, $\Upsilon(3S)$ and $\Upsilon(4S)$.

monium case, the spectral function in the vicinity of each peak can be fitted with a skewed Breit–Wigner distribution, allowing for the extraction of both the binding energy and the decay width. For bottomonium, the first two peaks are much more clearly resolved than in the charmonium case, enabling more precise fits, particularly at low temperatures. In contrast, the $\Upsilon(4S)$ state does not survive in the medium, and its corresponding peak is only present in the vacuum.

The binding energy, obtained from the position of the peak, is shown in Figure 7. Similarly to charmonium, the binding energy of bottomonium states decreases with increasing temperature. As expected, more weakly bound states dissociate at lower temperatures: the $\Upsilon(1S)$ survives up to higher temperatures than the $\Upsilon(2S)$, which in turn persists longer than the $\Upsilon(3S)$.

This hierarchy is evident in Figure 7, where states with larger initial binding energies extend over a wider temperature range. As the binding energy approaches the potential barrier, the corresponding peak becomes unresolvable, signaling the onset of dissociation.

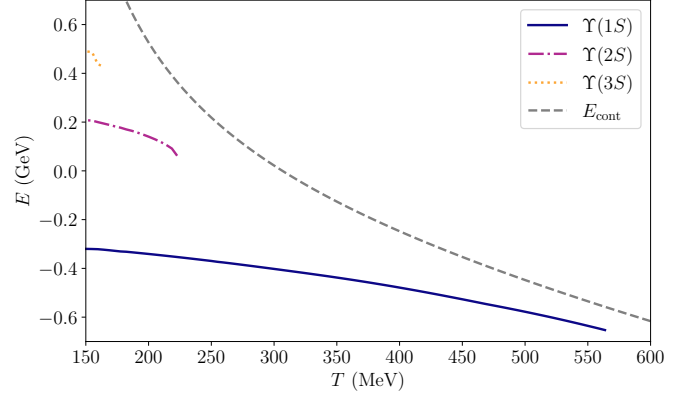


Figure 7: Binding energy for the different species of bottomonium at finite temperature: $\Upsilon(1S)$ (solid blue line), $\Upsilon(2S)$ (dash-dot magenta line), and $\Upsilon(3S)$ (dotted orange line). The potential barrier is also shown (dashed gray line).

Moreover, increasing the temperature leads to a broadening of the peaks, corresponding to an increase in the decay width. The decay width is therefore a monotonically increasing function of temperature, as shown in Figure 8.

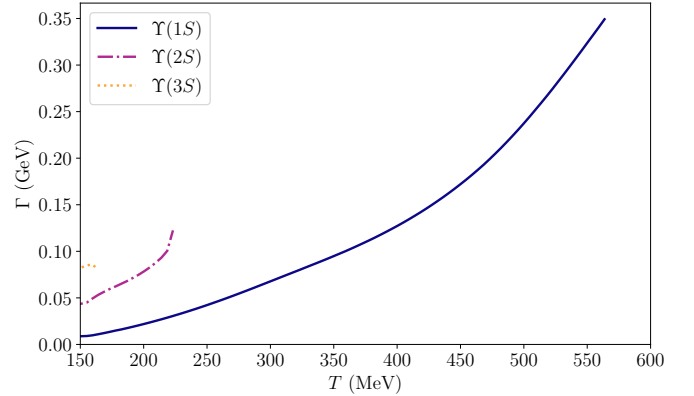


Figure 8: Decay width for the different species of bottomonium at finite temperature: $\Upsilon(1S)$ (solid blue line), $\Upsilon(2S)$ (dash-dot magenta line), and $\Upsilon(3S)$ (dotted orange line).

From this analysis, one can estimate the dissociation temperatures of the different bottomonium states. Ordered from most to least tightly bound, they are approximately

$$T_{\Upsilon(1S)} \approx 564 \text{ MeV}, \quad T_{\Upsilon(2S)} \approx 223 \text{ MeV}, \quad T_{\Upsilon(3S)} \approx 164 \text{ MeV}.$$

The $\Upsilon(4S)$ state dissociates at temperatures below the critical temperature, $T_c \approx 155 \text{ MeV}$, and therefore does not form within the medium. This provides an upper bound for its dissociation temperature, $T_{\Upsilon(4S)} < 155 \text{ MeV}$.

4. Survival probability

4.1. Suppression-only scenario

For a quarkonium state produced at time t_0 and traversing a QGP that cools according to Bjorken hydrodynamics [16], $T(t) = T_0 (t_0/t)^{1/3}$, the survival probability can easily be determined through the decay width

$$S(t_0, t) = \exp\left[-\int_{t_0}^t d\tau \Gamma(T(\tau))\right]. \quad (8)$$

If the initial temperature $T_0 > T_d$, the state is not formed; otherwise Eq. (8) applies from the formation time t_0 until the freeze-out time t_f defined by $T(t_f) = T_c$, around the phase transition value.

4.2. Lindblad framework and recombination

The inclusion of recombination is modeled by assuming that heavy quarks move non-relativistically around their center of mass and that Λ_{QCD} is larger than the binding energy. At finite temperature, the potential is modified by the medium. However, since the in-medium potential only captures the time-ordered correlator of the heavy quark–antiquark pair, a complete description of bound-state populations requires treating quarkonium as an open quantum system and following the evolution of its density matrix.

In the case $T \gg E$, where T is the temperature of the medium and E corresponds to the binding energy of the state that would conform the system, the evolution of the density matrix ρ is given by a Lindblad equation [6, 8, 7, 9]:

$$\frac{d\rho}{dt} = -i[H, \rho] + \sum_n (C_n \rho C_n^\dagger - \frac{1}{2}\{C_n^\dagger C_n, \rho\}), \quad (9)$$

where H is the Hamiltonian of the $Q\bar{Q}$ pair and the C_n are collapse operators describing transitions between color configurations and interactions with medium gluons.

The associated effective non-Hermitian Hamiltonian is

$$H_{\text{eff}} = H - \frac{i}{2} \sum_n C_n^\dagger C_n, \quad (10)$$

where $\text{Im} V(r) = -\frac{1}{2} \sum_n C_n^\dagger C_n$. With this redefinitions, the Lindblad equation can be written as

$$\frac{d\rho}{dt} = -iH_{\text{eff}}\rho + i\rho H_{\text{eff}}^\dagger + \sum_n C_n \rho C_n^\dagger. \quad (11)$$

Note that the development done in the previous section, focused on the Schrödinger equation with a non-Hermitian Hamiltonian, is equivalent to neglecting the last term on (11). This last term is the only one that takes into account the possibility of the regeneration of the bound-state wavefunction.

To compute uncorrelated recombination from the Lindblad equation [11], several assumptions are introduced. First, the heavy quark–antiquark system is described by a Markovian Lindblad equation, where the medium induces decoherence

and transitions between different states. We work in the dilute heavy-quark limit, considering only binary interactions and neglecting higher-order correlations. Unbound heavy quarks are assumed to be uncorrelated and locally thermalized with the medium (molecular chaos). In addition, an adiabatic approximation is used, meaning that the effective Hamiltonian and jump operators evolve slowly compared to the intrinsic timescales of the bound states, which allows one to define survival probabilities and recombination rates. It is important to note that this derivation differs slightly from the one in [11]. We make use of the non-Hermitian adiabatic theorem of [17], which states that at large times any initial state gets converted to the state with the smallest decay width. Since we are studying the fundamental state and we expect that to be also the “less decaying state”, the overall conclusion is the same; the bound state of the effective Hamiltonian at time t is mapped to the bound state of the Hamiltonian at time t' . Finally, recombination is assumed to be rare, so the population of unbound heavy quarks remains approximately constant during the evolution.

Following the derivation in [11], we project the Lindblad equation onto the bound-state subspace $P_b = \sum_i |i\rangle\langle i|$ and free subspace P_f . The probability per unit time for a stochastic jump from a free $Q\bar{Q}$ state to the bound state $|1S\rangle$ through channel n is

$$R_n = Z_{t,n} \text{Tr}[\rho_{t,n} \rho_f], \quad (12)$$

where the target density matrix and its normalization are

$$\rho_{t,n} = \frac{C_n^\dagger P_b C_n}{Z_{t,n}}, \quad Z_{t,n} = \text{Tr}[C_n C_n^\dagger P_b]. \quad (13)$$

Assuming that free heavy quarks are uncorrelated and thermalized (molecular chaos), their Wigner distribution is

$$W_f(\mathbf{R}, \mathbf{r}, \mathbf{P}, \mathbf{p}) = Z_f N^2 e^{-\frac{p^2}{4MT} - \frac{p^2}{M}}, \quad Z_f^{-1} = V^2 \left(\frac{MT}{2\pi}\right)^3, \quad (14)$$

where M is the heavy-quark mass, V the medium volume, and $N = N_Q = N_{\bar{Q}}$ the number of free heavy quarks. Substituting into Eq. (12) and using the Wigner transform leads to

$$R_{1S}(t) = \frac{Z_{t,1S} N^2}{V \left(\frac{MT}{4\pi}\right)^{3/2}} \int \frac{d^3 p}{(2\pi)^3} e^{-\frac{p^2}{MT}} W_{t,1S}(\mathbf{p}), \quad (15)$$

where $W_{t,1S}(\mathbf{p})$ is the target Wigner distribution. Following Ref. [11], we approximate $W_{t,1S} \approx W_{1S}$, the Wigner distribution of the bare bound-state wave function obtained by solving the Schrödinger equation in the previous section. We note that in the high temperature limit the above integral equals 1. We will use the high-temperature approximation from now on.

In Ref. [11], we have assumed that the normalization factor $Z_{t,1S}$ is equal to the thermal decay width of the state $Z_{t,1S}(T) = \Gamma_{1S}(T)$. This assumption relies on the fluctuation-dissipation theorem, which is only valid when the heavy quarks are fully thermalized. In fact, further corrections are needed for more realistic applications in heavy-ion collisions. In transport approaches [18], this is typically handled by introducing a relaxation factor which modulates the gain term in the rate equation,

$$\mathcal{R}(t) = 1 - \exp\left(-\int_{t_0}^t d\tau / \tau_Q^{\text{therm}}\right), \quad (16)$$

where τ_Q^{therm} represents the kinetic relaxation time of the heavy quark distributions, i.e., the time that the heavy quarks take to equilibrate within the medium. For charm quarks, it can be approximated by $\tau_c^{therm} \approx 4$ fm [19, 20]. Taking the relaxation time as proportional to the quark mass, the corresponding bottom quark's relaxation time is $\tau_b^{therm} \approx 12$ fm.

Therefore, we define the high temperature limit of (15) multiplied by the relaxation factor (16),

$$R(t) = \frac{Z_{t,1S} N^2}{V \left(\frac{MT}{4\pi}\right)^{3/2}} \mathcal{R}(t), \quad (17)$$

which is what we will use for phenomenological applications. We note that this is different from what we do for the $X(3872)$ in our previous paper [11], where the high temperature limit is only taken when made explicit and the relaxation factor never taken into account.

The contribution from coalescence to the probability for observing state $1S$ at freeze-out time t_f is, in the adiabatic approximation [11, 21],

$$N_{1S}^{recomb}(t_f) = \int_0^{t_f} dt S(t_f, t) R(t), \quad (18)$$

where $S(t_f, t)$ is the survival probability between times t and t_f computed from Eq. (8). The adiabatic approximation is valid when the bound-state energy levels change slowly compared to the time scale of a quantum jump, i.e., when

$$\frac{|i|\dot{V}|j\rangle|^2}{(E_i - E_j)^4} \ll 1 \quad \forall i \neq j. \quad (19)$$

This inequality holds for both J/ψ and $\Upsilon(1S)$ across the temperature range $[T_c, T_d]$.

5. Phenomenology in Pb–Pb collisions

One of the standard ways to quantify medium effects on particle production is the nuclear modification factor, R_{AA} . This observable is defined as the ratio between the particle yield in nucleus-nucleus collisions with mass number A , N^{AA} , and the yield in proton-proton collisions, N^{pp} , normalized by the number of binary nucleon-nucleon collisions N_{coll} expected in the nuclear interaction:

$$R_{AA} = \frac{N^{AA}}{N^{pp} N_{coll}}. \quad (20)$$

In the absence of nuclear effects, $N^{AA} = N^{pp} N_{coll}$ and the nuclear modification factor equals 1 by construction.

When initial cold nuclear matter (CNM) effects are taken into account, the nuclear yields are modified. Among these, the shadowing of the nuclear parton distribution functions (nPDFs) is the dominant contribution, see details of our implementation in [22, 11]. In this case, one can write:

$$N_{CNM}^{AA} = N_{coll} S^{sh} N^{pp}, \quad (21)$$

where S^{sh} corresponds to the shadowing factor.

In the presence of the medium the yield gets modified due to suppression and coalescence effects. Recalling the notation for the survival probability from (8) and the regeneration factor from (17), the full nuclear yield for one particle species is taken to be

$$N^{AA} = N_{CNM}^{AA} S(t_0, t_f) \Theta(T_d - T_0) + \int_{t_0}^{t_f} dt R(t) S(t, t_f) \Theta(T_d - T), \quad (22)$$

where $\Theta(x)$ is the Heaviside step function and T_d is the dissociation temperature of the species.

In Eq. (22), two distinct contributions can be identified: the initially produced particles, which are suppressed from the initial time t_0 up to the freeze-out time t_f , and the regenerated particles, which are suppressed from their formation time $t > t_0$ until t_f . The overall suppression in Eq. (22) is implemented through two mechanisms: the survival probability, which accounts for the effect of the imaginary part of the potential (i.e., Landau damping), and a Heaviside step function, introduced to model a sharp Debye screening at temperatures above T_d .

The full nuclear modification factor can be calculated by introducing Eq. (22) into Eq. (20). In the next subsections it will be computed for different quarkonia states.

In a realistic heavy-ion collision the temperature is not spatially uniform. We account for this by applying the survival probability locally at each transverse position \mathbf{x}_\perp , using the initial temperature profile $T_0(\mathbf{x}_\perp)$ from the model of Ref. [22].

5.1. Phenomenological inputs

The following ingredients are needed to evaluate the nuclear modification factor:

Medium evolution. We use Bjorken expansion with initial conditions $T_0 = 500$ MeV and $t_0 = 0.6$ fm, appropriate for Pb–Pb collisions at $\sqrt{s_{NN}} = 5.02$ TeV. The transverse temperature profile and the number of binary collisions N_{coll} are obtained from a Glauber model supplemented with the shadowing model of Ref. [22].

Initial open-charm and open-bottom production. The initial number of free charm (bottom) quarks is estimated from binary scaling, $N_{Q\bar{Q}}^{(0)} = N_{coll} \sigma_{pp \rightarrow Q\bar{Q}} / \sigma_{pp}$. We use the ALICE measurements $d\sigma_{pp \rightarrow c\bar{c}}/dy|_{|y|<0.5} = 1.165$ mb and $d\sigma_{pp \rightarrow b\bar{b}}/dy|_{|y|<0.5} = 34.5$ μ b at $\sqrt{s_{NN}} = 5.02$ TeV [23, 24].

pp baseline cross sections. For J/ψ we use the ALICE midrapidity cross section $d\sigma_{J/\psi}^{pp}/dy|_{y=0} = 5.64$ μ b at $\sqrt{s_{NN}} = 5.02$ TeV [25], including prompt production only. For the $\Upsilon(1S)$ we use the CMS measurement at $\sqrt{s_{NN}} = 5.02$ TeV [26], $d\sigma_{\Upsilon(1S)}^{pp}/dy|_{y=0} = 60.2$ nb.

Cold nuclear matter effects. CNM effects are modeled as shadowing using the framework in Ref. [22].

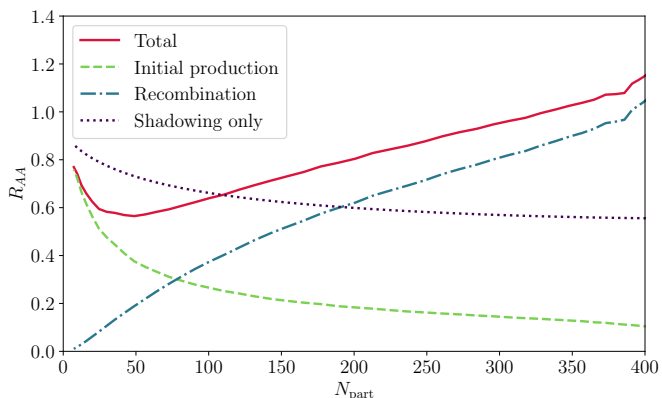


Figure 9: Nuclear modification factor R_{AA} of the J/ψ in Pb–Pb collisions at $\sqrt{s_{NN}} = 5.02$ TeV. The dotted curve shows only cold nuclear matter effects (shadowing); the dashed curve adds suppression from the complex Gauss-law potential; the dash-dot curve shows the recombination contribution alone; and the solid curve gives the total result.

5.2. Results for J/ψ

Figure 9 shows our prediction for $R_{AA}^{J/\psi}$ in Pb–Pb collisions at $\sqrt{s_{NN}} = 5.02$ TeV as a function of N_{part} , including both suppression and recombination contributions.

The J/ψ displays a sizeable recombination contribution in central collisions ($N_{\text{part}} \gtrsim 200$), driven by the relatively large charm-quark multiplicity at LHC energies. This recombination partially compensates the suppression, leading to a total R_{AA} around unity, significantly larger than the suppression-only result. The p_T -integrated prediction is dominated by low- p_T coalescence, consistent with the well-known regeneration picture for J/ψ at the LHC [27, 28].

5.3. Results for $\Upsilon(1S)$

Figure 10 shows the corresponding prediction for $R_{AA}^{\Upsilon(1S)}$. In contrast to the J/ψ case, the recombination contribution to the $\Upsilon(1S)$ is strongly suppressed. The bottom-quark multiplicity at LHC energies is roughly two orders of magnitude smaller than the charm-quark multiplicity, so the N^2/V factor in Eq. (15) is dramatically reduced. The total R_{AA} of the $\Upsilon(1S)$ is therefore dominated by suppression, with only a minor correction from coalescence.

5.4. Comparison to experimental data

In Figure 11, we show our results for the nuclear modification factors of both J/ψ and $\Upsilon(1S)$ compared to the experimental data available from ALICE [25] and CMS [26, 29]. The agreement is reasonable, considering the lack of fitting parameters in our approach where the relaxation times are taken from the literature [19, 20] for J/ψ and extrapolated for the Υ following the mass difference.

6. Summary and conclusions

We have applied the Lindblad-driven open quantum system framework to the production of the conventional quarkonium

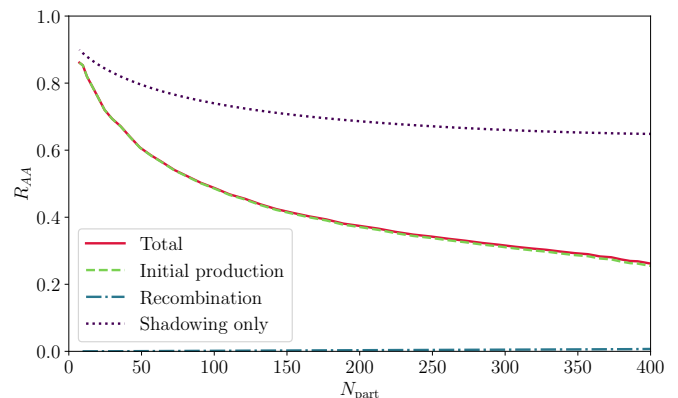


Figure 10: Nuclear modification factor R_{AA} of the $\Upsilon(1S)$ in Pb–Pb collisions at $\sqrt{s_{NN}} = 5.02$ TeV. Curves and symbols as in Fig. 9. The recombination contribution is significantly smaller than for the J/ψ due to the much smaller bottom-quark multiplicity, and it becomes barely visible.

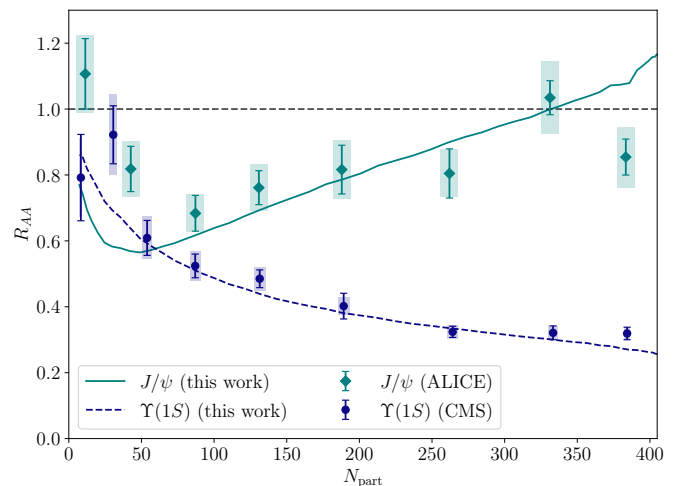


Figure 11: Nuclear modification factor R_{AA} of the J/ψ and $\Upsilon(1S)$ in Pb–Pb collisions at $\sqrt{s_{NN}} = 5.02$ TeV. Experimental data from ALICE [25] and CMS [26, 29] are shown for comparison.

ground states J/ψ and $\Upsilon(1S)$ in Pb–Pb collisions at $\sqrt{s_{NN}} = 5.02$ TeV. Our approach proceeds as follows: First, we use the Gauss-law model of Lafferty and Rothkopf [5], which provides a single-parameter ($m_D(T)$) parametrization of both $\text{Re } V$ and $\text{Im } V$, the complex in-medium potential. By solving the Schrödinger equation with the complex potential and extracting the imaginary part of the corresponding Green’s function, we obtain the quarkonium spectral functions for both charmonium and bottomonium across a wide range of temperatures. The spectral shape directly encodes the in-medium properties of each state: the peak positions, after subtracting the masses of the two constituent quarks, yield the binding energies, the half-widths at half-maximum give the thermal decay widths, and the temperature at which a given peak merges into the continuum defines the dissociation temperature. From this analysis we find $T_{J/\psi} \approx 372$ MeV and $T_{\psi(2S)} \lesssim 155$ MeV for charmonium, and

$T_{\Upsilon(1S)} \approx 564$ MeV, $T_{\Upsilon(2S)} \approx 223$ MeV, $T_{\Upsilon(3S)} \approx 164$ MeV and $T_{\Upsilon(4S)} < 150$ MeV for bottomonium, with the thermal decay widths entering directly the survival probability under Bjorken expansion.

Following Ref. [11], we derive a coalescence model directly from the Lindblad equation by projecting the stochastic jump operators onto the bound-state subspace. Under the adiabatic approximation, the recombination rate $R_{1S}(t)$ is proportional to N^2/V , where N is the number of free heavy quarks in the medium volume V , and is computed using the vacuum wave functions obtained from the Schrödinger equation together with the fluctuation-dissipation theorem, which identifies the normalization factor $Z_{i,1S}$ with the thermal decay width $\Gamma_{1S}(T)$. We further correct the number of heavy quark-antiquark pairs available for recombination in the medium by a modulation due to the finite relaxation time of heavy quarks. The time-dependent recombination yield is then given by Eq. (17), where each regenerated state is subsequently suppressed by the survival probability from its formation time until freeze-out. At LHC energies, the charm-quark multiplicity is large enough to make recombination a significant contribution for the J/ψ in central collisions, partially compensating the suppression and bringing the total R_{AA} into agreement with ALICE and CMS measurements. In contrast, the bottom-quark multiplicity is roughly two orders of magnitude smaller, so the N^2/V factor is dramatically reduced and recombination remains negligible for the $\Upsilon(1S)$, whose R_{AA} is therefore governed almost entirely by suppression.

The Lindblad framework provides a unified, first-principles-inspired treatment of both suppression and recombination, with a direct microscopic link between the complex potential and the observable yield. Unlike phenomenological approaches in which suppression and regeneration are modeled independently and then combined by hand, the present framework derives both mechanisms from a single equation of motion for the density matrix of the heavy quark–antiquark pair. The imaginary part of the in-medium potential enters directly as the generator of decoherence and decay, determining the thermal decay widths and hence the survival probability, while the same jump operators that drive dissociation also govern the recombination rate. This internal consistency ensures that suppression and regeneration are not treated as competing corrections but as two complementary manifestations of the same underlying dynamics. The resulting description is therefore not only more theoretically grounded than traditional transport models, but also more predictive: once the complex potential is fixed, here through the Gauss-law model, all medium effects on the quarkonium yield follow without additional free parameters. We regard this as a significant step toward a truly first-principles description of quarkonium production in heavy-ion collisions.

Acknowledgements. NA, EGF and VLP are supported by European Research Council project ERC-2018-ADG-835105 YoctoLHC, by Xunta de Galicia (CIGUS Network of Research Centres), by European Union ERDF, and by the Spanish Research State Agency under projects

PID2023152762NB—I00 and CEX2023-001318-M financed by MICIU/AEI/10.13039/501100011033. The work of MAE has been supported by the Maria de Maeztu excellence program under project CEX2024-001451-M, and by project PID2022-136224NB-C21 funded by MICIU/AEI/10.13039/501100011033, and by grant 2021-SGR-249 of Generalitat de Catalunya. MAE acknowledges the hospitality of the MITP during the workshop Exotic Quarkonia in Heavy-ion Collisions and the discussions with its participants. VLP has been supported by Xunta de Galicia under project ED481A2022/286.

References

- [1] Tetsuo Matsui and Helmut Satz. J/ψ Suppression by Quark-Gluon Plasma Formation. *Phys. Lett. B*, 178:416, 1986. doi: 10.1016/0370-2693(86)91404-8.
- [2] Anton Andronic et al. Heavy-flavour and quarkonium production in the LHC era: from proton-proton to heavy-ion collisions. *Eur. Phys. J. C*, 76(3):107, 2016. doi: 10.1140/epjc/s10052-015-3819-5.
- [3] Mikko Laine, Owe Philipsen, Paul Romatschke, and Markus Tassler. Real-time static potential in hot QCD. *JHEP*, 03:054, 2007. doi: 10.1088/1126-6708/2007/03/054.
- [4] A. Beraudo, J.-P. Blaizot, and C. Ratti. Real and imaginary-time Q anti-Q correlators in a thermal medium. *Nucl. Phys. A*, 806:312, 2008. doi: 10.1016/j.nuclphysa.2008.03.001.
- [5] David Lafferty and Alexander Rothkopf. Improved Gauss law model and in-medium heavy quarkonium at finite density and velocity. *Phys. Rev. D*, 101(5):056010, 2020. doi: 10.1103/PhysRevD.101.056010.
- [6] Yukinao Akamatsu and Alexander Rothkopf. Stochastic potential and quantum decoherence of heavy quarkonium in the quark-gluon plasma. *Phys. Rev. D*, 85:105011, 2012. doi: 10.1103/PhysRevD.85.105011.
- [7] Nora Brambilla, Miguel Angel Escobedo, Joan Soto, and Antonio Vairo. Quarkonium suppression in heavy-ion collisions: an open quantum system approach. *Phys. Rev. D*, 96(3):034021, 2017. doi: 10.1103/PhysRevD.96.034021.
- [8] Jean-Paul Blaizot and Miguel Angel Escobedo. Quantum and classical dynamics of heavy quarks in a quark-gluon plasma. *JHEP*, 06:034, 2018. doi: 10.1007/JHEP06(2018)034.
- [9] Nora Brambilla, Miguel Angel Escobedo, Joan Soto, and Antonio Vairo. Heavy quarkonium suppression in a fireball. *Phys. Rev. D*, 97(7):074009, 2018. doi: 10.1103/PhysRevD.97.074009.

- [10] Néstor Armesto, Miguel Angel Escobedo, Elena G. Ferreira, and Víctor López-Pardo. A potential approach to the X(3872) thermal behavior. *Phys. Lett. B*, 854:138760, 2024. doi: 10.1016/j.physletb.2024.138760.
- [11] Néstor Armesto, Miguel Ángel Escobedo, Elena G. Ferreira, and Víctor López-Pardo. Lindblad-driven recombination of the X(3872) tetraquark. 2026.
- [12] Albert M Sirunyan et al. Evidence for X(3872) in Pb-Pb Collisions and Studies of its Prompt Production at $\sqrt{s_{NN}} = 5.02$ TeV. *Phys. Rev. Lett.*, 128(3):032001, 2022. doi: 10.1103/PhysRevLett.128.032001.
- [13] Estia Eichten, Kurt Gottfried, Toichiro Kinoshita, Kenneth D. Lane, and Tung-Mow Yan. Charmonium: The Model. *Phys. Rev. D*, 17:3090, 1978. doi: 10.1103/PhysRevD.17.3090.
- [14] Antonio Pineda. Determination of the bottom quark mass from the Upsilon(1S) system. *JHEP*, 06:022, 2001. doi: 10.1088/1126-6708/2001/06/022.
- [15] Yannis Burnier, Mikko Laine, and Mikael Vepsalainen. Heavy quarkonium in any channel in resummed hot QCD. *JHEP*, 01:043, 2008. doi: 10.1088/1126-6708/2008/01/043.
- [16] James D. Bjorken. Highly Relativistic Nucleus-Nucleus Collisions: The Central Rapidity Region. *Phys. Rev. D*, 27:140, 1983. doi: 10.1103/PhysRevD.27.140.
- [17] Parveen Kumar, Yuval Gefen, and Kyrylo Snizhko. General theory of slow non-Hermitian evolution. 2 2025.
- [18] Loic Grandchamp, Ralf Rapp, and Gerald E. Brown. In medium effects on charmonium production in heavy ion collisions. *Phys. Rev. Lett.*, 92:212301, 2004. doi: 10.1103/PhysRevLett.92.212301.
- [19] Taesoo Song, Kyong Chol Han, and Che Ming Ko. Charmonium production from nonequilibrium charm and anticharm quarks in quark-gluon plasma. *Phys. Rev. C*, 85:054905, 2012. doi: 10.1103/PhysRevC.85.054905.
- [20] Biaogang Wu and Ralf Rapp. Charmonium Transport in Heavy-Ion Collisions at the LHC. *Universe*, 10(6):244, 2024. doi: 10.3390/universe10060244.
- [21] Albert Messiah. *Quantum Mechanics*. Dover Publications, 1999. Two volumes bound as one.
- [22] Miguel Angel Escobedo and Elena G. Ferreira. Simple model to include initial-state and hot-medium effects in the computation of quarkonium nuclear modification factor. *Phys. Rev. D*, 105(1):014019, 2022. doi: 10.1103/PhysRevD.105.014019.
- [23] Shreyasi Acharya et al. Charm-quark fragmentation fractions and production cross section at midrapidity in pp collisions at the LHC. *Phys. Rev. D*, 105(1):L011103, 2022. doi: 10.1103/PhysRevD.105.L011103.
- [24] Shreyasi Acharya et al. Measurement of beauty and charm production in pp collisions at $\sqrt{s} = 5.02$ TeV via non-prompt and prompt D mesons. *JHEP*, 05:220, 2021. doi: 10.1007/JHEP05(2021)220.
- [25] Shreyasi Acharya et al. Inclusive J/ψ production at mid-rapidity in pp collisions at $\sqrt{s} = 5.02$ TeV. *JHEP*, 10:084, 2019. doi: 10.1007/JHEP10(2019)084.
- [26] Albert M Sirunyan et al. Suppression of Excited Υ States Relative to the Ground State in Pb-Pb Collisions at $\sqrt{s_{NN}} = 5.02$ TeV. *Phys. Rev. Lett.*, 120:142301, 2018. doi: 10.1103/PhysRevLett.120.142301.
- [27] Peter Braun-Munzinger and Johanna Stachel. (Non)thermal aspects of charmonium production and a new look at J/ψ suppression. *Phys. Lett. B*, 490:196, 2000. doi: 10.1016/S0370-2693(00)00991-6.
- [28] Robert L. Thews, Martin Schroedter, and Johann Rafelski. Enhanced J/ψ production in deconfined quark matter. *Phys. Rev. C*, 63:054905, 2001. doi: 10.1103/PhysRevC.63.054905.
- [29] Albert M Sirunyan et al. Measurement of prompt and nonprompt charmonium suppression in PbPb collisions at 5.02 TeV. *Eur. Phys. J. C*, 78(6):509, 2018. doi: 10.1140/epjc/s10052-018-5950-6.